R-matrix calculations of electron collisions with a lithium atom at low energies

Michal Tarana* and Roman Čurík
J. Heyrovský Institute of Physical Chemistry of the ASCR, Dolejškova 2155/3, 182 23 Prague 8, Czech Republic

(Received 20 July 2018; revised manuscript received 17 November 2018; published 18 January 2019)

R-matrixcalculations of the electron collisions with a lithium atom at energies below the 3*s* excitation threshold are presented. The $^1S^e$, $^3S^e$, and $^1P^o$ phase shifts calculated in the near-threshold energy range are in excellent agreement with previous theoretical studies. The threshold behavior of the $^3P^o$ phase shift is accurately analyzed along with the resonance located at the scattering energy ∼60 meV. The phase shifts and cross sections calculated here show two resonances below the 3*s* threshold that have not been previously reported.

DOI: 10.1103/PhysRevA.99.012708

I. INTRODUCTION

Ultralong-range Rydberg molecules, for the first time theoretically predicted by Greene *et al.* [1], are very exotic systems in which one atom in its ground state interacts with another atom in its highly excited Rydberg state with the distance of the nuclei varying between 10^2 and 10^4 a.u. [1–3]. The existence and character of the electronic bound states of these molecules are determined by the low-energy interaction between the Rydberg electron and the neutral atom in the ground state. Typically, this interaction is approximated by the *s*-wave zero-range Fermi pseudopotential [4] and its *p*-wave extension [3,5] or by the finite-range model potential [2]. Both models are constructed using the *s*-wave and *p*-wave phase shifts of the corresponding electron-atom scattering process at energies below the lowest threshold of the electronic excitation.

So far, the ultracold quantum gases, particularly those consisting of the heavier alkali metals, have provided the most suitable environment for the experimental realization and study of the ultralong-range Rydberg molecules [6–8]. The design and interpretation of these experiments require accurate theoretical models of the long-range Rydberg molecules and, therefore, accurate phase shifts of the electron collisions with the alkali-metal atoms at the low scattering energies [9]. Recently, Schmid *et al.* [10] proposed an experiment to study the ion-atom scattering in the ultracold regime based on the photoionization of the Li-Li ultralong-range Rydberg molecules. Although the low-energy e^--Li scattering has been studied both theoretically [11–14] and experimentally [14–16], the demand for accurate and consistent data by the experimental research groups dealing with the ultralong-range Rydberg molecules involving lithium justifies us to revisit this topic using very accurate contemporary computational methods.

The *ab initio* calculations by Norcross [12] provide a very accurate characterization of the $^1S^e$ and $^3S^e$ electron collisions with the lithium atoms at very low scattering energies between 0.1 and 68 meV. The phase shifts calculated in this energy range are fitted to the modified effective range theory (MERT) [17] and the accurate values of the singlet and triplet scattering lengths are obtained.

However, Norcross [12] calculated the $^1P^o$ and $^3P^o$ scattering phase shifts only for three values of the scattering energies between 0.13 and 0.4 eV. Although the extrapolation of the $^1P^o$ phase shifts towards very low energies using the MERT is adequate, it is questionable in the $^3P^o$ case since the lowest $^3P^o$ resonance is located below the interval where the scattering calculations were performed.

The low-energy e^--Li scattering was also studied by Burke and Taylor [11] using the close-coupling (CC) expansion where the states of the neutral target were approximated by the Hartree-Fock wave functions. The ranges of the scattering energies at which the phase shifts are calculated in Refs. [11,12] overlap between 0.1 and 0.9 eV. Although the $^1S^e$, $^1P^o$, and $^3P^o$ phase shifts calculated by Burke and Taylor [11] are in excellent agreement with those published by Norcross [12] in this energy interval, their $^3S^e$ phase shift raises more rapidly with decreasing scattering energy than in Ref. [12]. As a result, each of these two works [11,12] predicts the Ramsauer-Townsend minimum at different energies. Moreover, the low-energy $^3P^o$ phase shift and cross section published by Burke and Taylor [11] show a clear resonance at ∼0.06 eV. However, the character of the cross section below this resonance suggests that the calculations by Burke and Taylor [11] yield different threshold behavior than that predicted by Norcross [12].

The experimental research of the electron-atom scattering becomes increasingly more challenging with decreasing collision energies. Jaduszliwer *et al.* [16] measured the total e^--Li scattering cross section above the $2p$ threshold. The excitation cross sections were measured by Leep and Gallagher [15]. However, to our best knowledge, no experimental results have been published for the scattering energies below the lowest excitation threshold. Therefore, in order to compare the present calculations with the experiment, it was necessary to perform the *R*-matrix computations for the energies above the $2p$ excitation threshold. Another theoretical study in this energy region was published by Moores [13], who utilized the CC approach involving the five lowest states of the target.

*michal.tarana@jh-inst.cas.cz

The goal of this paper is to introduce such a model of the e^--Li collisions that provides accurate results from very low scattering energies to the $3s$ threshold of the electronic excitation. Parametrization of the phase shifts at very low scattering energies presented in this paper provides the data necessary for the research of the ultralong-range Rydberg molecules and other phenomena where the electrons interact with the neutral lithium atom at low energies. Extension of the calculations towards the energies above the $2p$ excitation threshold uncovers new resonances that were not mentioned in the previously published papers. The reason why they do not appear in the previously published studies [13,15] is that the energy grids at which the cross sections were calculated [13] and measured [15,16] were not fine enough to resolve the corresponding narrow structures.

Atomic units are used throughout the paper unless stated otherwise. Since lithium is a very light element, no spin-orbit interaction or other relativistic effects are considered in this work. The rest of this paper is organized as follows: Sec. II deals with the representation of the Li^+ core by a model potential, and the parameters of the R-matrix calculations are discussed in Sec. III. The phase shifts and cross sections are analyzed in Sec. IV.

II. MODEL POTENTIAL OF Li^+

In the calculations discussed below, the target atom is represented by its valence electron in the presence of the spherically symmetric potential $V_{l_1}(r)$ that models the closed-shell core of Li^+. This model potential is constructed individually for every angular momentum l_1 of the valence electron. It is optimized in such way that the energies of the low-lying bound states supported by $V_{l_1}(r)$ coincide with the energies of the ground and low excited states of the lithium atom.

The form of $V_{l_1}(r)$ used in this work is

$$V_{l_1}(r) = -\frac{1 + 2\exp(-a_{l_1} r) + b_{l_1} r \exp(-c_{l_1} r)}{r} - \frac{\alpha_d}{2r^4} W_6(\rho_{l_1}, r), \quad (1)$$

where a_{l_1}, b_{l_1}, c_{l_1}, and ρ_{l_1} are the parameters to be optimized, $\alpha_d = 0.189$ a.u. is the polarizability of the Li^+ core [18], and

$$W_n(r_c, r) = 1 - \exp[-(r/r_c)^n] \quad (2)$$

is the cutoff function regularizing the potential at the origin. Equation (1) is a generalization of the potential employed by Pan *et al.* [19] that is l_1 independent and the polarization part of the potential vanishes less rapidly with decreasing value of r than in $V_{l_1}(r)$ constructed in this work. A very similar l_1-dependent model potential was developed to represent the Li^+ core by Marinescu *et al.* [20] in their research of the dispersion coefficients for the alkali-metal dimers. Generally, in the research of the interactions between electrons in the continuum and neutral atoms or positive ions, the cationic cores have been very successfully modeled by this form of the potential (see Refs. [19–21] as well as Ref. [22] and references therein).

The set of parameters a_{l_1}, b_{l_1}, c_{l_1}, and ρ_{l_1} was optimized using the nonlinear least-squares method independently for $l_1 = 0, 1, 2$. The accurate theoretical [23] and experimental [24] energies of the five lowest states with respect to the ionization threshold for every $l_1 = 0, 1, 2$ were taken as the data to be matched by the model. In every iteration, it was necessary to diagonalize the one-particle Hamiltonian operator $\hat{H}_{l_1} = \hat{K} + V_{l_1}(r)$, where $\hat{K}$ is the operator of the kinetic energy. The match of the obtained eigenenergies ε_{nl} with the experimental data then determined the adjustments of $V_{l_1}(r)$ in the next iteration. Note that the index n plays a role of the principal quantum number as known in the atomic physics. In the calculations presented here, $\hat{H}_{l_1}$ was represented by the radial basis set consisting of 2000 B splines [25] of the sixth order that spanned the sphere with radius 240 a.u. This size of the sphere was chosen with respect to the fact that the classical turning point of the highest fitted bound state is at ∼95 a.u. A sufficient radial interval beyond this limit allowed for the accurate exponential decrease of the wave function and eliminated the artifacts of the finite box. In order to guarantee accurate representation of the atomic orbitals by the B-spline basis set in every iteration of the nonlinear optimization as well as accurate matrix elements of $V_{l_1}(r)$, the radial box was split into three subintervals with different spatial densities of the B splines. The splitting points of these subintervals along with corresponding numbers of B splines in each of them are listed in the top section of Table I. The knot sequence defined in every subinterval was equidistant. The size of each segment and corresponding part of the basis set reflect the different character of the wave functions near the Coulomb singularity, in the classically allowed region and beyond the classical turning point of the highest fitted bound state. Further increase of the number of the B splines in any of these subintervals had negligible effect on the quality of the optimized model potential.

TABLE I. Distribution of the B-spline basis functions among the subintervals of the radial box used in the calculations. The top section shows the radial segments of the box used in the nonlinear optimization of $V_{l_1}(r)$, and the section in the center corresponds to the subintervals defined in the two-electron R-matrix calculations in the inner region. The number of B splines used in the R-matrix propagation in the outer region (that was not further split into subintervals) is listed in the bottom section. All the corresponding knot sequences were equidistant and the order of all the B splines was 6.

	Radial subinterval (a.u.)	Number of B splines
Optimization of $V_{l_1}(r)$	[0, 1/3]	80
	[1/3, 8.5]	820
	[8.5, 240]	1100
R matrix (inner region)	[0, 1/3]	30
	[1/3, 2]	30
	[2, 120]	94
R matrix (propagation)	[120, 2700]	1200

The comparison of the top and middle sections in Table I shows that the numbers of the basis functions used in the nonlinear optimization of $V_{l_1}(r)$ are significantly larger than the corresponding numbers of the B splines utilized in the scattering calculations discussed below. The reason

TABLE II. Optimized values of the parameters of $V_{l_1}(r)$ in Eq. (1) for Li^+.

	$l_1 = 0$	$l_1 = 1$	$l_1 = 2$
a_{l_1}	10.655	2.734	25.915
b_{l_1}	3.397	46.621	7.562
c_{l_1}	2.821	10.493	18.200
ρ_{l_1}	0.375	1.294	1.258

is that the nonlinear least-squares method requires a sufficiently flexible basis set to represent the nonphysical wave functions that appear in the iterations where the convergence criteria are not met. Those functions can have much more complicated character than the optimized atomic orbitals and scattering wave functions represented by the radial basis in the *R*-matrix calculations. However, their corresponding (and unrealistic) energies need to be computed reliably. The values of the parameters optimized to represent Li^+ in the *R*-matrix calculations discussed below are listed in Table II. The model potential $V_{l_1}(r)$ with these parameters yielded less than 1 meV deviation of the calculated energy levels from the lowest five experimental values [24] for every $l_1 \leqslant 2$.

The best match between the experimental energies of the *s* states and the spectrum of the $\hat{H}_0$ was achieved when the lowest eigenvalue ε_{10} was omitted from the optimization of $V_{l_1}(r)$ and the second eigenenergy ε_{20} was compared with the ground state of the lithium atom. This is related to the fact that the $1s$ orbital in lithium is doubly occupied by the core electrons and the lowest *s* orbital available for the valence electron is $n = 2$ that possesses one radial node. As a result, $\hat{H}_0$ supports one very deeply bound corelike nonphysical state with the energy $\varepsilon_{10} = -2.0069$ a.u. with respect to the ionization threshold. This orbital is very compact; its classical turning point is located at ∼0.75 a.u. The eigenenergies ε_{n0} above this state very accurately correspond to the experimental energy levels of the lithium atom [24].

For $l_1 > 2$, the energies of the lithium bound states are so close to the corresponding levels of the hydrogen atom that with very good approximation the Coulomb potential $-1/r$ can be taken instead of $V_{l_1}(r)$.

Although it is not the main objective of this work, it is interesting to mention that $V_{l_1}(r)$ also yields accurate energies of the excited states higher than those to which $V_{l_1}(r)$ was optimized. Figure 1 shows the quantum defects $\mu_{l_1}(\varepsilon)$ calculated for $V_{l_1}(r)$ [26]. Its good correspondence to the experimental results [27,28] (note the order-of-magnitude decrease of $\mu_{l_1}(\varepsilon)$ with increasing value of l_1) implies that $V_{l_1}(r)$ also correctly models the *s*, *p*, and *d* Rydberg states of the Li atom.

The aim of the extensive radial basis set utilized in the optimization discussed above is to eliminate the effects of the finite basis set as much as possible and to provide the model potential that is independent of the basis set. Note that this approach is different from the method frequently used in quantum chemistry to represent the atomic cores by the potentials. In such calculations, mainly based on the Gaussian basis sets, the parameters of the potential are optimized for

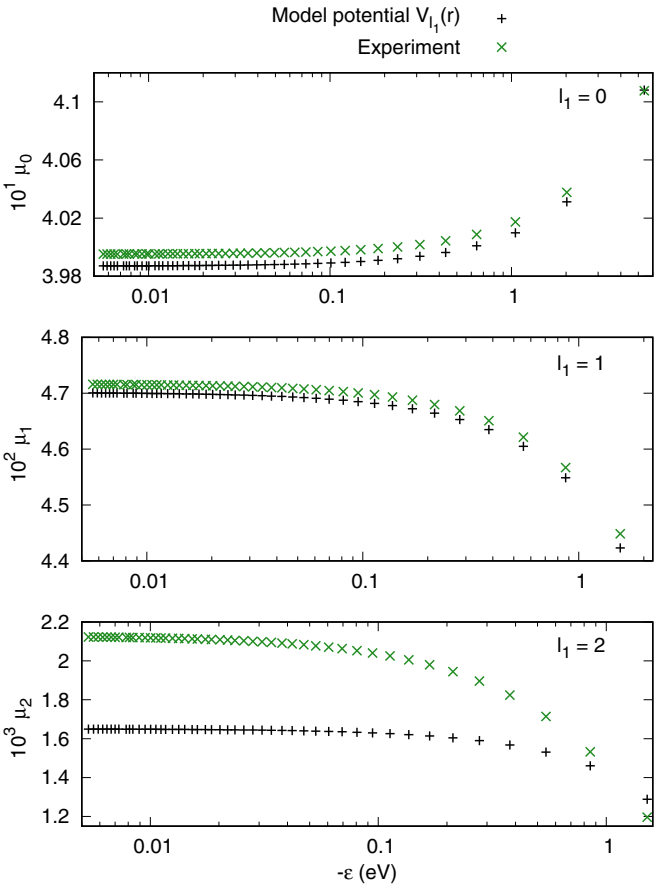

FIG. 1. Quantum defects $\mu_{l_1}(\varepsilon)$ of Li as functions of the negative energy ε (logarithmic scale) taken with respect to the ionization threshold. The top, center, and bottom panels show the results for $l_1 = 0, 1, 2$, respectively. The values obtained using the model potential $V_{l_1}(r)$ in Eq. (1) and parameters from Table II (+) are compared with the experimental results published by Goy *et al.* [27] for $l_1 = 0, 1$ and by Lorenzen and Niemax [28] for $l_1 = 2$ (×).

one specific basis set that becomes part of the model along with the optimized potential (see Ref. [29] and references therein).

In the calculations of the electron collisions with lithium at low energies, Norcross [12] also used a model potential to represent the Li^+ core. The parameters of the scaled Thomas-Fermi potential [30] with additional polarization term were optimized to accurately reproduce the energies of the two lowest eigenstates of the lithium atom. The Thomas-Fermi potential was also utilized by Moores [13] to calculate the $1s$ core wave functions of Li^+. The valence orbitals of the neutral lithium were obtained from the e^--Li^+ scattering calculations. On the other hand, Burke and Taylor [11], in their work, represented the lithium atom by the Hartree-Fock wave function and constrained the $1s$ orbital to be doubly occupied in all the terms considered in the following CC expansion of the scattering wave function.

In the two-electron calculations, the approximation of the noble-gas-like core by the model potential $V_{l_1}(r)$ can be corrected by including the dielectronic term introduced by

Chisholm and Öpik [31] in the two-electron Hamiltonian:

$$V_{\rm diel}(\rho_c, r_1, r_2, \theta_{1,2}) = -\frac{\alpha_d}{r_1^2 r_2^2}[W_6(\rho_c, r_1)W_6(\rho_c, r_2)]^{1/2} P_1(\cos\theta_{12}) - \frac{\alpha_q}{r_1^3 r_2^3}[W_{10}(\rho_c, r_1)W_{10}(\rho_c, r_2)]^{1/2} P_2(\cos\theta_{12}), \quad (3)$$

where r_1 and r_2 are the radial coordinates of the first and second electron, respectively, $\theta_{1,2}$ is the angle between their position vectors, $P_n(x)$ is the nth Legendre polynomial, ρ_c is the cutoff parameter, and α_q is the quadrupole polarizability of the core. This term describes the interaction between the valence and scattering electrons via the dipole and quadrupole moments induced on the core. Although this correction becomes more important for the heavier alkali metals, it was included in the R-matrix calculations presented in this work with $\alpha_q = 0.037$ a.u. [32]. The value of the cutoff parameter $\rho_c = 4.03$ a.u. was chosen in such way that the electron affinity of Li^- obtained by the diagonalization of the two-electron Hamiltonian discussed in Sec. III including the correction (3) coincides with the accurate experimental value of 0.617 eV [33]. The electron affinity calculated using the value of ρ_c mentioned above is 0.620 eV.

III. *R*-MATRIX CALCULATIONS

The scattering calculations discussed below were performed using the R-matrix computer program by Tarana and Čurík [34] originally designed to calculate the electronic states of the long-rang Rydberg molecules. The notation introduced in Ref. [34] was adopted in this section. The reader is also referred there for the definitions of the open and closed one-particle wave functions and two-electron configurations (see also Ref. [22]). Only the inner-region part of the program by Tarana and Čurík [34] was used in this work. The outer-region code was developed independently and it consists of the propagation of the R matrix in the long-range potentials of the target [19,35] as well as of the construction of the K matrix, T matrix, and calculation of the phase shifts and cross sections [36–38].

The radius of the R-matrix sphere was set to $r_0 = 120$ a.u. This allows for a smooth transition between the short-range two-electron and long-range one-electron interactions. The long-range effects become particularly important at the scattering energies near the $2s$ threshold. This is the energy range from which the accurate values of the MERT parameters can be obtained. Since the full interaction of the electrons with each other as well as with the Li^+ core is considered in the inner region, the treatment of the long-range effects inside this relatively large sphere is not restricted only to the potential due to the static dipole polarizability of the target. It also includes the effects of the higher multipoles of the ground and excited states. Similarly large spheres were used by Pan *et al.* [19] in their R-matrix calculations of the photodetachment of Li^-.

The set of 154 radial B splines of the sixth order was used inside the R-matrix sphere to represent the closed and open single-particle wave functions [34].

The radial dimension of the inner region was split into three subintervals in similar way as the box used for the nonlinear optimization of the model potential. The knot sequence defined in each of them was equidistant. The boundaries of each segment and corresponding numbers of B splines are listed in the middle section of Table I.

For every one-electron angular momentum $l \leqslant 7$, the 25 lowest closed orbitals were included in the closed part of the ansatz for the two-electron wave function.

The energies of the highest included closed s orbital and p orbital were 4.909 and 4.983 eV above the Li ionization threshold, respectively. With increasing angular momentum, the energy of the highest included orbital in every l gradually increased towards 6.793 eV above the ionization threshold for $l = 7$.

All possible excitations involving these orbitals were included in the construction of the corresponding configuration-interaction (CI) Hamiltonian matrix $\underline{H'}$. The lowest 6, 6, 5, 3, and 1 closed orbitals among the s, p, d, f, and g states, respectively, were included in the open part of the two-electron wave-function ansatz [34] as the scattering channels. This extensive basis set ensures very accurate treatment of all the correlation and polarization effects. Our tests showed that further augmentation of the basis set has negligible impact on the calculated scattering quantities.

The CI matrix $\underline{H'}$ representing the two-electron Hamiltonian in the inner region (including the dielectronic term (3) and Bloch operator [22,34,36,39]) was diagonalized and using the eigenvalues (R-matrix poles) E_k, the R matrix was calculated as

$$R_{\bar{j}\bar{j}'}(E) = \frac{1}{2}\sum_k \frac{w_{\bar{j}k} w_{\bar{j}'k}}{E_k - E}, \quad (4)$$

where E is the total energy of the e^--Li system and $w_{\bar{j}k}$ are the surface amplitudes—projections of the kth eigenstate of $\underline{H'}$ on the target state n with the angular momentum l_1 and on the partial wave l_2 of the scattered electron [22,34,36,39]. The multi-index $\bar{j} = \{n, l_1, l_2\}$ denotes the scattering channel.

Since the total angular momentum L, total spin S, and total parity $P = (-1)^{l_1+l_2}$ of the e^--Li system are good quantum numbers, the scattering calculation can be performed independently for each LSP symmetry and the cross sections calculated in this way can be summed to obtain the results that can be compared with the experiments.

It is worth mentioning at this point that the spectrum of $\underline{H'}$ includes a set of nonphysically low R-matrix poles E_k. This is an artifact of the very low-lying compact orbital with energy ε_{10} discussed in Sec. II. In the eigenstates corresponding to these low-lying R-matrix poles, the configurations where the compact $1s$-like orbital is singly or doubly occupied are dominant and not strongly coupled to the configurations involving the higher valence orbitals. Since, in addition, this corelike target state was not included in the CC expansion as the scattering channel, there are no surface amplitudes $w_{\bar{j}k}$ associated with it. As a result, these nonphysically low-lying eigenstates of $\underline{H'}$ do not appear in the pole expansion (4) of the R matrix and they do not affect the results of the scattering calculations.

This work is dealing with the kinetic energies of the incident electron $\epsilon \leqslant 3.3$ eV where only the $2s$ and $2p$ channels are open. The $2p$ channel opens at the energy $\epsilon = 1.848$ eV above the $2s$ threshold and the threshold of the $3s$ channel is located at $\epsilon = 3.373$ eV. Although all the remaining higher channels included in the scattering calculations are closed, their presence ensures the accurate treatment of the long-range e^--Li interaction in the outer region represented by the transition dipole moments coupling the target states [19,39]. In spite of the large R-matrix box, the propagation of the R matrix [35] in the long-range tail of the lithium potential to the distance 2700 a.u. from the center was necessary to obtain converged phase shifts at energies below 1 meV suitable for the calculation of the MERT parameters. The R-matrix propagation [35] was performed using the basis set consisting of 1200 B splines of the sixth order equidistantly distributed between the inner-region boundary $r_0 = 120$ a.u. and the distance 2700 a.u. (see also the bottom section of Table I) beyond which the interaction between the target and the projectile was neglected.

One way to assess the representation of the e^--Li interaction by the dipole potentials coupling the target states outside the R-matrix sphere is to calculate the static dipole polarizability α_{20} of the ground state of the target from the dipole moments used as the open and closed channels in the present R-matrix propagation [40]:

$$\alpha_{nl_1} = 2 \sum_{\substack{l_1' = l_1 \pm 1 \\ n' \neq n}} \frac{|\langle \psi_{n'l_1'} | z | \psi_{nl_1} \rangle|^2}{\varepsilon_{n'l_1'} - \varepsilon_{nl_1}}, \tag{5}$$

where $|\psi_{n'l_1'}\rangle$ and $|\psi_{nl}\rangle$ are the eigenstates of the target and the matrix element in the numerator of Eq. (5) is the z component of the corresponding transition dipole moment. This equation yields polarizability of the lithium atom in the ground state $\alpha_{20} = 163.7$ a.u. that is in excellent agreement with previously published theoretical and experimental values varying between 163.74 and 164.19 a.u. (see Ref. [41] and references therein). The contribution from the $2s \rightarrow 2p$ term to the series (5) represents more than 99% of the calculated value and all the higher terms are its small corrections.

The R matrix propagated to the distance 2700 a.u. from the center is used to match the linear combination of the regular and irregular free-particle solutions of the Schrödinger equation in the open channels [36]. This yields the K matrix and its subsequent diagonalization provides the scattering phase shifts. The scattering amplitudes and cross sections are then calculated using the standard methods of the multichannel scattering theory [37]. It is not necessary to consider the closed channels in the matching of the free-particle solutions and to perform any elimination of the closed channels [22]. In this case, the energy range around the threshold where the closed channels influence the results is negligible.

Our test R-matrix calculations performed for two different R-matrix spheres with radii $r_0 = 120$ a.u. and $r_0 = 130$ a.u. showed that when the R-matrix propagation in the outer region was performed to the distance 2700 a.u., the dependence of the phase shifts and cross sections on r_0 was negligible.

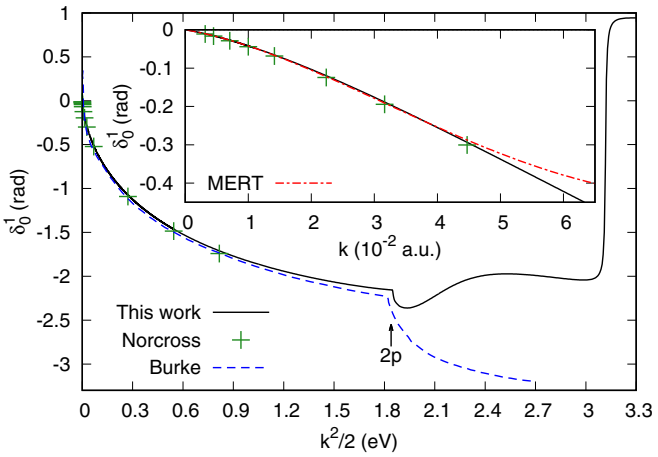

FIG. 2. $^1S^e$ phase shift as a function of the kinetic energy of the scattered electron. The results calculated in this work (solid black line) are compared with previously published data by Norcross [12] (+) and Burke and Taylor [11] (blue dashed line). The inset shows the detail of the phase shifts as a function of the momentum of the incident electron k in the range 0–0.06 a.u. (corresponding to the interval of the kinetic energies 0–57 meV). The red dash-dotted line is the MERT [17] fit of the current results ($A_1 = 2.81$).

IV. RESULTS

A. Phase shifts

In this section, the dependence of the phase shifts $\delta_{l_2}^{2S+1}(\epsilon)$ on the kinetic energy of the incident electron $\epsilon = k^2/2$ is presented as follows: Below the $2p$ threshold, $\delta_{l_2}^{2S+1}(\epsilon)$ is a single phase shift corresponding to the partial wave l_2 of the scattered electron according to the total LSP symmetry of the e^--Li system. Above the $2p$ threshold, $\delta_{l_2}^{2S+1}(\epsilon)$ is the sum of all the eigenphases obtained by the diagonalization of the multichannel K matrix. The superscript $2S+1$ denotes the multiplicity of the e^--Li system. Since the parity $P = (-1)^{l_1+l_2}$ and since the electron collisions with lithium in its excited states are not a subject of this work, it is sufficient to deal only with those LSP symmetries where $P = (-1)^L$ as only in these the colliding electron is coupled with the ground state of the target. Therefore, it is not necessary to use parity index to denote the phase shifts in different LSP symmetries.

The $^1S^e$ phase shift calculated using the R-matrix method is plotted in Fig. 2. Its comparison with the results calculated by Norcross [12] shows an excellent agreement for the energy range between 0.1 meV and 0.8 eV.

The rapid decrease at very low scattering energies is the consequence of the $^1S^e$ bound state of Li^-. The low-energy s-wave phase shifts calculated in this work can be parametrized by the MERT [17]:

$$\frac{\tan \delta_0^{2S+1}(k)}{k} = -A_{2S+1} - \frac{\pi\beta^2 k}{3} - \frac{4}{3} A_{2S+1} \beta^2 k^2 \ln(1.23\beta k) - \frac{1}{2} r'_{0,2S+1} A_{2S+1}^2 k^2 + \frac{1}{3}\pi\beta^2 k^3 \left[A_{2S+1}^2 + \frac{7\beta^2}{117} \right], \tag{6a}$$

TABLE III. Summary of the scattering lengths A and parameters B in Eq. (9) calculated for different LSP symmetries and their comparison with values previously published by Norcross [12]. Parameters of the resonances E_r and Γ were obtained by fitting the calculated phase shifts to Eq. (7b). The configuration with the dominant contribution to the resonance is listed in the last column.

LSP	MERT		Resonances					
symmetry	R-matrix	Norcross [12]	E_r (eV)	Γ (meV)	P_0	P_1	P_2	Configuration
$^1S^e$	$A_1 = 2.81, r_{01} = 129.1$	$A_1 = 3.04$	3.117	11	1.932	−7.946		$3s^2$
$^3S^e$	$A_3 = -7.45, r_{03} = 0.40$	$A_3 = -7.12$						
$^1P^o$	$B_1 = -1.85$	$B_1 = -1.69$						
$^3P^o$	$B_3 = 0.236$	$B_3 = 1.992$	0.062	68	0.504	−69.888	340.589	$2s2p$
			3.285	45	0.107	2.367		$3s3p$

where

$$\frac{1}{2}r'_{0,2S+1} = \frac{1}{2}r_{0,2S+1} + \frac{\pi\beta}{3} - \frac{\pi\beta^3}{3A^2_{2S+1}}, \tag{6b}$$

the parameter A_{2S+1} is the scattering length, $r_{0,2S+1}$ denotes the effective range, and $\beta^2 = \alpha_{20}$.

This fit yields the scattering length $A_1 = 2.81$ and corresponding effective range $r_{01} = 129.1$. While the optimized value of r_{01} is sensitive to the energy interval taken for the nonlinear fit, the scattering length A_1 does not considerably change. Moreover, if the ground-state polarizability α_{20} is treated as a fitting parameter, its value from the inner-region calculations (5) is reconstructed and the scattering length A_1 remains unchanged.

The $^1S^e$ scattering length obtained from the R-matrix calculations discussed here is slightly lower than the value 3.04 reported by Norcross [12]. A possible reason for this subtle difference may lie in the fact that the R-matrix propagation utilized in this work allows for stable evaluation of $\delta^1_0(\epsilon)$ at lower energies than those considered by Norcross [12]. As a result, the MERT parametrization performed at lower collision energies can also yield a slightly different value of A_1. As can be seen in the inset of Fig. 2, the MERT parametrization [17] of the $^1S^e$ phase shift considerably deviates from the R-matrix results at scattering energies above 17 meV.

Below the $2p$ excitation threshold, the R-matrix calculations also show an agreement with the results obtained by Burke and Taylor [11]. The discrepancy increases at the scattering energies above the $2p$ threshold due to the terms in the CC expansion involving the target orbitals with higher energies and angular momenta that are not included in Ref. [11]. However, they are necessary for accurate representation of the interaction between the incident electron and the valence electron of the target. This issue of the truncated CC expansion in Ref. [11] is not specific only for the $^1S^e$ scattering but it is common for all the LSP symmetries.

Another structure in the calculated $^1S^e$ phase shifts that can be seen in Fig. 2 around 3.1 eV is the narrow Feshbach resonance below the $3s$ threshold with the dominant configuration $3s^2$. It can be very accurately fitted to the Breit-Wigner formula [42]

$$\delta(\epsilon) = \delta_{\rm bg}(\epsilon) + \delta_{\rm res}(\epsilon), \tag{7a}$$

where $\delta_{\rm bg}(\epsilon)$ is the background phase shift slowly varying with the energy,

$$\delta_{\rm res}(\epsilon) = \arctan\left[-\frac{\Gamma/2}{\epsilon - E_r}\right], \tag{7b}$$

where energy E_r is the position of the resonance and Γ is its width. Since Eqs. (7) can be applied to the resonances in any LSP symmetry, the indices l and $2S+1$ are omitted from the notation of the resonant and background phase shifts. When $\delta_{\rm bg}(\epsilon)$ is assumed to be a slowly varying function of the energy,

$$\delta_{\rm bg}(\epsilon) = P_0 + P_1\epsilon, \tag{8}$$

the fit yields $E_r = 3.117$ eV and $\Gamma = 11$ meV. The optimized values of P_0 and P_1 are listed in Table III. The analysis of the CI configurations contributing to the resonant wave function revealed that this resonance has Feshbach character with the dominant configuration $3s^2$. To our best knowledge, this resonance has not been reported in any previously published papers dealing with the e^--Li collisions. Due to its symmetry, this resonance is expected to appear in the two-photon detachment spectrum of Li^- at the photon energy ∼0.072 a.u. A similar spectrum was calculated by Glass *et al.* [43]. However, the highest photon energy considered in that work was 0.05 a.u.

Figure 3 shows the comparison of the $^3S^e$ phase shifts calculated using the R-matrix method with previously published results. Like in the case of the singlet discussed above, the data obtained in this work are in very good agreement with those calculated by Norcross [12]. As a result, the energy at which $\delta^3_0(\epsilon)$ changes from positive to negative (that corresponds to the Ramsauer-Townsend minimum in the cross section) calculated in this work also matches very well with the value obtained by Norcross [12]. Fitting of the calculated phase shifts to MERT [17] yields the scattering length $A_3 = -7.45$ and the effective range $r_{03} = 0.40$ that is consistent with the previously published value $A_3 = -7.12$ [12]. As can be seen in the inset of Fig. 3, the MERT parametrization of $\delta^3_0(\epsilon)$ is valid at energies below 5 meV. The steep increase of the s-wave phase shift at very low energies followed by the rapid drop is characteristic for the scattering systems that possess the virtual state [37] (represented by a pole of the S matrix on the negative imaginary axis in the complex momentum plane) with sufficiently small energy.

The reason behind the deviation of the $^3S^e$ phase shifts calculated by Burke and Taylor [11] from the results presented in this work and those obtained by Norcross [12] is that

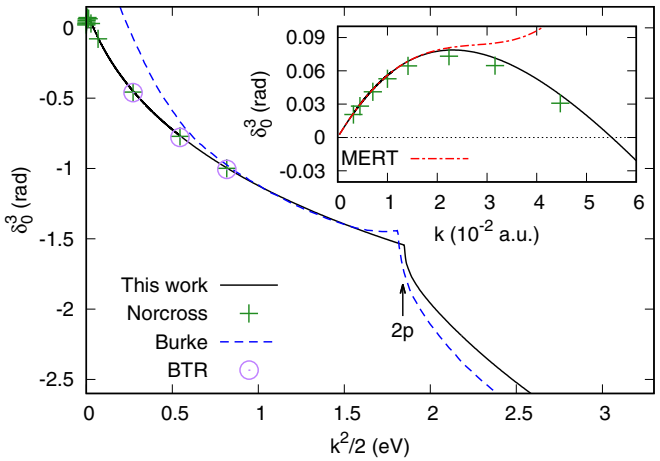

FIG. 3. $^3S^e$ phase shift as a function of the kinetic energy of the scattered electron. The meaning of the plotted lines and points is identical to Fig. 2. The circles (○) represent the results of Norcross [12] obtained after the orthogonality correction to Burke's procedure. The red dash-dotted line is the MERT fit of the current results ($A_3 = -7.45$).

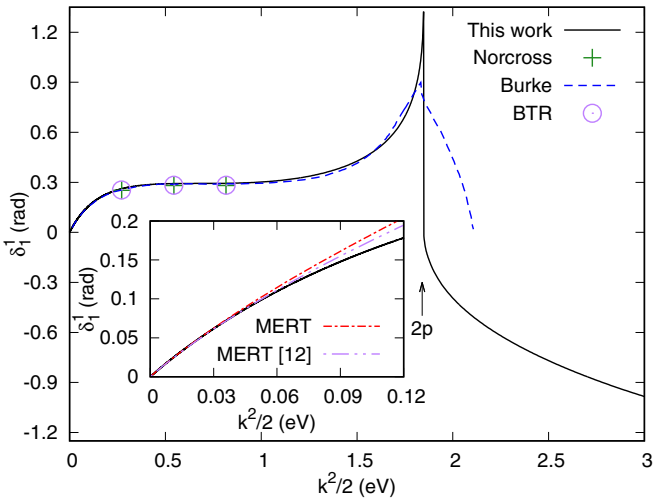

FIG. 4. $^1P^o$ phase shift as a function of the kinetic energy of the colliding electron. The data are displayed with the same symbols as in Fig. 3. The inset shows the detail of the phase shifts in the range below 120 meV. The red dash-dotted line corresponds to the MERT fit of the current results ($B_1 = -1.85$), and the violet dash-dot-dotted line is the MERT with $B_1 = -1.69$ taken from Ref. [12].

the CC method, as formulated by Burke and Taylor [11], does not guarantee that the continuum wave functions of the colliding electron are orthogonal to the Hartree-Fock orbitals of the target [44]. When Norcross [12,44] introduced this orthogonality into the CC equations formulated by Burke and Taylor [11] as the additional constraint (circles denoted as BTR in Fig. 3), the phase shifts calculated in this way became consistent with those obtained using other approaches discussed in this work. This orthogonality issue is common to all the LSP symmetries discussed here, except for the $^1S^e$ scattering [44]. It is another limitation of the computational method used in Ref. [11] in addition to the truncation of the CC expansion mentioned above.

The $^1P^o$ phase shifts calculated using the R-matrix method are in excellent agreement with the results of Norcross [12] at all three energy points where the latter are provided (see Fig. 4). In Ref. [12], these were extrapolated towards the low energies near the threshold using the p-wave MERT [45] as

$$\delta_1^{2S+1}(k) = \frac{\pi\beta^2 k^2}{15} + \frac{\beta^3 k^3}{9B_{2S+1}}, \tag{9}$$

with the value of the fitting parameter $B_1 = -1.69$. The parametrization of our R-matrix results at the scattering energies below 10 meV using Eq. (9) yields a similar value, $B_1 = -1.85$. As can be seen in the inset of Fig. 4, this parametrization fits the *ab initio* results for energies below 50 meV. In spite of the issue with the orthogonality of the continuum wave functions and target orbitals discussed above, at energies below the $2p$ threshold, the phase shifts obtained by Burke and Taylor [11] are in encouraging agreement with our R-matrix calculations and the orthogonality correction [12] does not considerably change the results. Rigorously, Eq. (9) above should contain an additional term $\sim k^3$ not involving β [45]. Its presence is dictated by the Wigner threshold law for the short-range interactions. Since only the whole coefficients in front of k^3 can be fitted and since β is constant, we used the form (9) in order to have like-to-like comparison with the MERT fit by Norcross [12].

Norcross [12] also performed the low-energy p-wave MERT extrapolation of the $^3P^o$ phase shift calculated at the same three energy points between 0.2 and 0.8 eV as in the $^1P^o$ symmetry and obtained the value of the fitting parameter $B_3 = 1.992$. However, the adequacy of this extrapolation can be called into question as there is a $^3P^o$ resonance below 100 meV that changes the threshold behavior of the phase shift and the MERT expansion may not be valid above this energy (see Fig. 5). The value optimized by fitting our R-

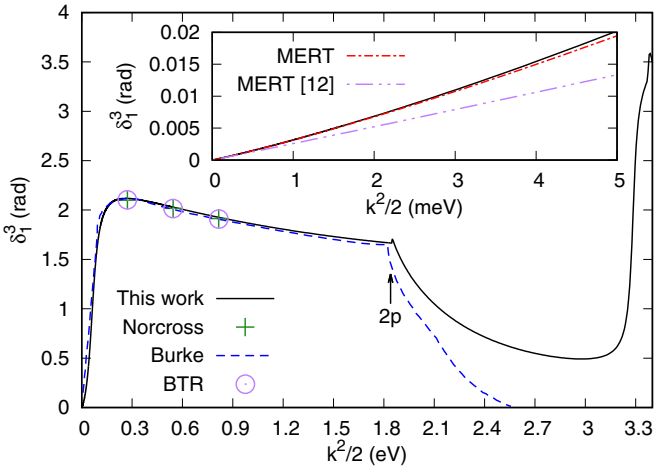

FIG. 5. $^3P^o$ phase shift as a function of the kinetic energy of the scattered electron. The data are displayed with the same symbols and lines as in Fig. 3. The inset shows the detail of the phase shifts in the range below 5 meV. The red dash-dotted line corresponds to the MERT fit of the current results ($B_3 = 0.236$), and the violet dash-dot-dotted line represents the MERT with $B_3 = 1.992$ taken from Ref. [12].

matrix results to Eq. (9) at energies sufficiently below this resonance is considerably smaller: $B_3 = 0.236$. As can be seen in the inset of Fig. 5, this parametrization is more consistent with the *ab initio* results than the parametrization in Ref. [12].

The lowest $^3P^o$ resonance is associated with the rapid increase of the phase shift below 0.3 eV in Fig. 5. It is a shape resonance with the dominant configuration $2s2p$. In general, the modification of the resonant character of the phase shift by the threshold law at low energies is determined by two factors: the analytical behavior of the scattering wave function near the origin and the asymptotic behavior of the scattering wave function at low energies. The energy ranges, where these factors play a role, can be different. The consequence of the first factor is that the resonances at sufficiently low energies cannot be parametrized by Eq. (7b). Instead, the generalization taking into account the energy dependence of the resonance width ($\Gamma(\epsilon) = \Gamma_0\epsilon^{3/2}$) and level shift is necessary (see the review [46] and references therein). The asymptotic character of the scattering wave function related to the long-range interaction implies that the low-energy phase shifts satisfy Eqs. (6) and (9) for $l_2 = 0$ and $l_2 > 0$, respectively, even when a resonance appears within the range of energies where the MERT is valid.

Our tests of multiple models that treat the interaction of the resonance with the threshold show that the phase shift $\delta_1^3(\epsilon)$ in the corresponding energy interval can be accurately fitted to Eqs. (7) assuming the near-threshold behavior of the background phase shift consistent with Eq. (9),

$$\delta_{\rm bg}(\epsilon) = P_0 + P_1\epsilon + P_2\epsilon^{3/2}, \tag{10}$$

where the value of $P_0 = -\delta_{\rm res}(0)$ is chosen so that $\lim_{\epsilon\to 0}\delta(\epsilon) = 0$, and P_1 and P_2 are the fitting variables. This optimization yields $E_r = 62$ meV and $\Gamma = 68$ meV. The optimized values of P_0, P_1, and P_2 are listed in Table III. This parametrization provides a numerically accurate model of the low-energy behavior of the $^3P^o$ phase shift suitable for the construction of related zero-range potentials [3,5].

Another $^3P^o$ resonance appears just below the $3s$ excitation threshold (see Fig. 5) and, assuming that $\delta_{\rm bg}(\epsilon)$ is linear [Eq. (8)], it can be parametrized using the Breit-Wigner formula (7) where $E_r = 3.285$ eV and $\Gamma = 45$ meV. This is a core-excited (Feshbach) resonance with dominant configuration $3s3p$.

The $^1D^e$ and $^3D^e$ phase shifts calculated in this study are plotted in Fig. 6 along with the results obtained by Burke and Taylor [11]. While the triplet phase shifts agree very well below the $2p$ threshold, the singlet results of Burke and Taylor [11] are, for energies above 1.2 eV, lower than those obtained from the *R*-matrix calculations presented here. The phase shift steeply raises above this energy, reaching the highest value above the $2p$ threshold. Like the low-energy $^3P^o$ resonance discussed in the text above, the fit of this resonance by the Breit-Wigner formula (7) is complicated by its interaction with the threshold. In this case, however, the resonant structure in the phase shifts reaches the energy regions both below and above the $2p$ threshold. Therefore, $\delta_{\rm bg}(\epsilon)$ has a different energy dependence below and above the $2p$ threshold. Since this resonance is relatively broad compared to the other resonances discussed above, the steep

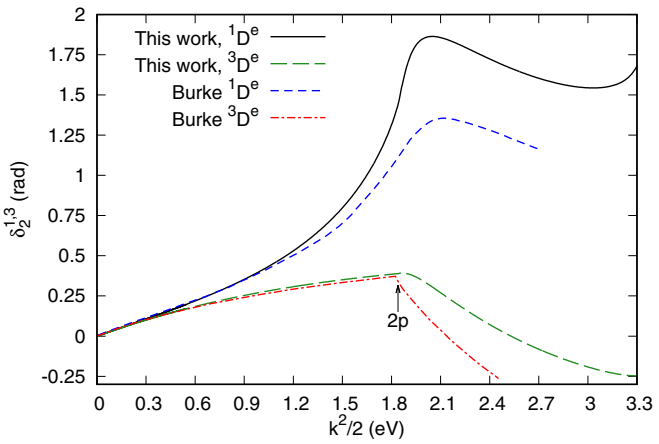

FIG. 6. $^1D^e$ and $^3D^e$ phase shifts calculated using the *R*-matrix method as functions of the kinetic energy of the colliding electron (solid black line and long-dashed green line, respectively) are compared with the $^1D^e$ and $^3D^e$ results calculated by Burke and Taylor [11] (short-dashed blue line and dot-dashed red line, respectively).

increase of the phase shift cannot be attributed only to $\delta_{\rm res}(\epsilon)$. This makes the values of E_r and Γ very sensitive to the form of $\delta_{\rm bg}(\epsilon)$ and to the energy range taken for the fit. Note that this resonance also appears in the two-photon detachment spectrum of Li^- calculated by Glass *et al.* [43].

In addition to the LSP symmetries discussed above, the *R*-matrix calculations were also performed for the higher total angular momenta of the e^--Li system up to $L = 5$ in both singlet and triplet. Corresponding phase shifts (not shown in this paper) are generally smaller than those for $L < 3$ presented above and there are no resonances in the energy interval below the $3s$ threshold. However, their inclusion in the calculation of the cross sections is necessary to achieve the convergence and agreement with the experimental results.

B. Cross sections

All the scattering cross sections presented in this section are averaged over the initial spin states and summed over the final spin states [38]. The integral cross sections for the elastic scattering calculated using the *R*-matrix method are plotted in Fig. 7. The dominant structure in the cross sections is the narrow peak located at 75 meV that corresponds to the low-lying $^3P^o$ resonance discussed above (see Fig. 5 and Table III). The change of the $^3S^e$ phase shift from positive to negative values shown in the inset of Fig. 3 is reflected in the elastic cross section as the Ramsauer-Townsend minimum located around 7 meV. As can be seen in Fig. 7, the resonance peak calculated in this work is in good agreement with that published by Burke and Taylor [11]. However, their calculation yields one more peak at lower energy. It is most likely an artifact caused by the nonorthogonality of the continuum wave functions on the target orbitals [44] that is particularly problematic in the $^3S^e$ scattering.

Another sharp peak in the elastic cross section occurs at the energy 1.84 eV where the $2p$ channel opens. It is a

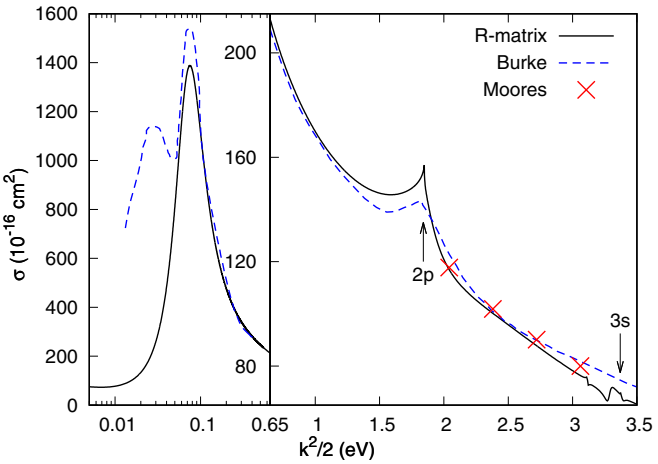

FIG. 7. Cross section of the elastic electron collisions with lithium calculated using the *R*-matrix method as a function of the kinetic energy of the colliding electron (solid black line) and its comparison with the results of the CC calculations [11] (blue dashed line) as well as with the theoretical results published by Moores [13] (×). The low-energy range is presented using the logarithmic energy scale.

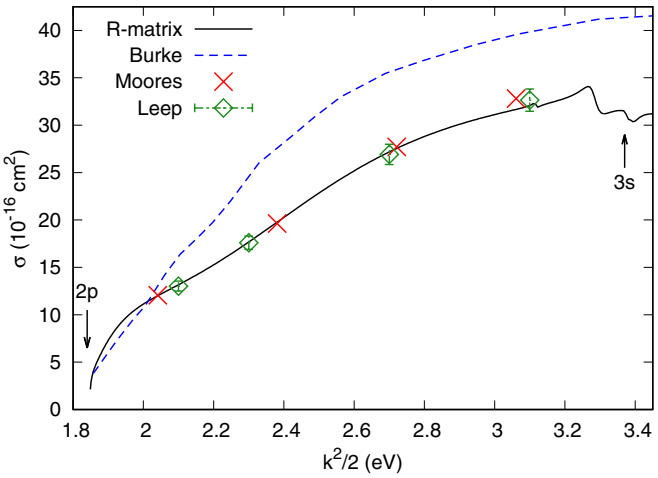

FIG. 8. Cross sections of the $2s \rightarrow 2p$ electronic excitation of lithium by electron impact at energies between the $2p$ and $3s$ threshold. The solid black line represents the *R*-matrix calculation presented in this work, and the blue dashed line is the result obtained by Burke and Taylor [11]. The theoretical cross section by Moores [13] (×) and experimental data by Leep and Gallagher [15] (◇) are plotted for comparison.

consequence of the $^1D^e$ resonance (see the corresponding phase shifts in Fig. 6) and very pronounced threshold behavior in the $^1P^o$ and $^3P^o$ symmetries (Wigner cusp). In order to obtain converged cross sections in this energy region, it is necessary to include all the total angular momenta of the e^--Li system up to $L = 4$ for both singlet and triplet configurations. The difference of the cross sections obtained from the *R*-matrix calculations discussed in this work and those reported by Burke and Taylor [11] corresponds to the discrepancy of the phase shifts discussed above. Figure 7 also shows the comparison with the elastic cross section calculated by Moores [13] who utilized the CC approach involving the five lowest states of the target. These results are in slightly better agreement with the *R*-matrix cross sections than those by Burke and Taylor [11] obtained using more limited CC expansion, although the elastic cross section calculated by Moores [13] decreases with the energy more slowly than our results presented here.

Although the $^1S^e$ and $^3P^o$ resonances located close to the $3s$ threshold are narrow (see Table III), our results plotted in Fig. 7 show that they do not dramatically change the magnitude of the cross sections. Due to a sparse energy grid at which Moores [13] evaluated the cross sections, these resonances do not appear in that theoretical study.

As can be seen in Fig. 8, our *R*-matrix calculations including the higher angular momenta and target orbitals with higher energies yield lower cross sections for the electronic excitation to the $2p$ state than the CC expansion of Burke and Taylor [11]. The excellent agreement with the results of Moores [13] and with the experimental data of Leep and Gallagher [15] shows that the five-state CC expansion [13] provides converged and quantitatively accurate results of the electronic excitation in the energy range between the $2p$ and $3s$ threshold. The difference between the *R*-matrix cross sections presented here, those calculated by Moores [13], and the measurements by Leep and Gallagher [15] is within very small uncertainties estimated by the authors of the experimental work [15].

The sum of the elastic and $2s \rightarrow 2p$ excitation cross section between the $2p$ and $3s$ thresholds is plotted in Fig. 9. The present results are lower than the total cross section reported by Burke and Taylor [11] and slightly lower than that published by Moores [13]. Out of all three theoretical results, the present *R*-matrix cross sections are closest to the experimental data observed by Jaduszliwer *et al.* [16] in the

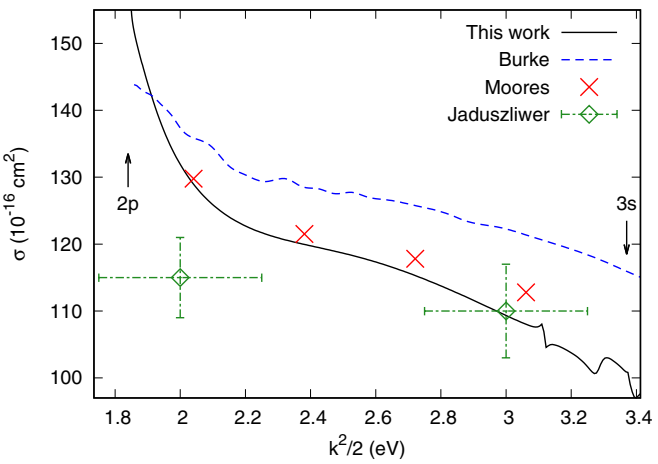

FIG. 9. Total cross section for the e^--Li collisions above the $2p$ threshold as a sum of the elastic and $2s \rightarrow 2p$ excitation cross sections plotted in Figs. 7 and 8, respectively. The solid black line represents the results of the *R*-matrix calculations, and the blue dashed line is the cross section calculated by Burke and Taylor [11]. The results by Moores [13] are represented by the red crosses (×) and the green diamonds (◇) are the experimental values measured by Jaduszliwer *et al.* [16].

energy region below the $3s$ threshold. Figure 9 shows that the experimental value at energy of 3 eV is in excellent agreement with the R-matrix calculations presented here, although the nearest value calculated by Moores [13] is also within the uncertainty interval estimated in Ref. [16]. It is not straightforward to address the difference that can be seen at the energy of 2 eV. It is well known that the crossed-beam scattering experiments become more challenging at lower collision energies. The energy profile of the incident electron beam becomes broader and it is more difficult to form a well-focused beam.

V. CONCLUSIONS

The aim of the present study is to provide accurate *ab initio* data for the e^--Li scattering that can be used for modeling ultralong-range Rydberg molecules containing the Li atom. In the first step, the atomic core of Li^+ is replaced by a model potential whose parameters are fitted to accurately reproduce the atomic excitation energies. By the very extensive size of the one-electron basis set we attempted to eliminate any impact of this basis on the model potential; i.e., the functional form of the potential should be considered independent of the basis set.

The optimized model potential is then used in the following two-electron R-matrix method developed by the authors [34] to compute the phase shifts for the total angular momentum up to $L = 5$ and for the collision energies up to the $3s$ excitation threshold. The phase shifts up to $L = 2$, in both singlet and triplet channels, are discussed in detail, while the higher L values are only used to obtain converged integral cross sections presented in this work.

Phase shifts for $L = 0$ ($^1S^e$ and $^3S^e$ symmetries) agree well with previous calculations of Norcross [12] and Burke and Taylor [11] up to the first excitation threshold. The low-energy tail of the latter data required a correction to properly incorporate orthogonality of the continuum states for the $^3S^e$ symmetry and it was carried out by Norcross [12]. The obtained low-energy MERT parameters can be considered as refinements of those published by Norcross [12]. For higher collision energies, our results deviate from those of Burke and Taylor [11]. Moreover, we report a narrow $3s^2$ Feshbach resonance at 3.117 eV located in $^1S^e$ symmetry.

Phase shifts for $L = 1$ are dominated by the $^1P^o$ resonance that was very well represented in calculations of Burke and Taylor [11] and omitted by Norcross [12]. The narrow character of the resonance allowed us to fit the phase shift as a sum of the threshold-law phase and the Breit-Wigner formula. The resulting MERT parameter B_3 disagrees with the one provided by Norcross [12] as the latter was determined from higher collision energies for which the $^1P^o$ resonance at 62 meV does not exist.

The resonance that can be seen in $^1D^e$ phase shifts is wider when compared to those in lower total angular momenta L. A strong background together with the presence of the $2p$ excitation threshold provides a very difficult situation for determination of the resonance parameters. Therefore, they are not given in the present study. Moreover, our results start to deviate from the calculations of Burke and Taylor [11] already well below the $2p$ excitation threshold.

The elastic as well as $2s \rightarrow 2p$ inelastic integral cross sections were calculated for the energies below the $3s$ excitation threshold. At very low energies, our results show the Ramsauer-Townsend minimum at 7 meV whereas in the calculations of Burke and Taylor [11], this minimum is disturbed by the presence of an additional low-energy peak. Above the $2p$ excitation threshold, the total cross section of Burke and Taylor [11] becomes gradually higher than in the present calculations, mainly due to higher $2s \rightarrow 2p$ electronic excitation cross sections. Our results in this case agree well with those by Moores [13]. Furthermore, out of all three calculations, the present data exhibit the best agreement with the experimental total cross sections [16].

The lack of any experimental data on the e^--Li scattering for collision energies under 2 eV strongly underlines the necessity for accurate theoretical results that could be utilized in the design of ultracold molecular experiments [10]. Moreover, we believe that the techniques reported here for the construction of the model potential replacing the atomic core can be also used for the heavier alkali-metal atoms.

ACKNOWLEDGMENTS

M.T. acknowledges the support of the Czech Science Foundation (Project No. P203/17-26751Y). The contributions of R.Č. were supported by the Czech Science Foundation (Grant No. 18-02098S).

[1] C. H. Greene, A. S. Dickinson, and H. R. Sadeghpour, Phys. Rev. Lett. **85**, 2458 (2000).
[2] A. A. Khuskivadze, M. I. Chibisov, and I. I. Fabrikant, Phys. Rev. A **66**, 042709 (2002).
[3] E. L. Hamilton, C. H. Greene, and H. R. Sadeghpour, J. Phys. B **35**, L199 (2002).
[4] E. Fermi, Nuovo Cimento **11**, 157 (1934).
[5] A. Omont, J. Phys. (Paris) **38**, 1343 (1977).
[6] V. Bendkowsky, B. Butscher, J. Nipper, J. P. Shaffer, R. Low, and T. Pfau, Nature (London) **458**, 1005 (2009).
[7] M. A. Bellos, R. Carollo, J. Banerjee, E. E. Eyler, P. L. Gould, and W. C. Stwalley, Phys. Rev. Lett. **111**, 053001 (2013).
[8] V. Bendkowsky, B. Butscher, J. Nipper, J. B. Balewski, J. P. Shaffer, R. Löw, T. Pfau, W. Li, J. Stanojevic, T. Pohl, and J. M. Rost, Phys. Rev. Lett. **105**, 163201 (2010).
[9] C. Bahrim, U. Thumm, and I. I. Fabrikant, Phys. Rev. A **63**, 042710 (2001).
[10] T. Schmid, C. Veit, N. Zuber, R. Löw, T. Pfau, M. Tarana, and M. Tomza, Phys. Rev. Lett. **120**, 153401 (2018).
[11] P. G. Burke and A. J. Taylor, J. Phys. B: At. Mol. Phys. **2**, 869 (1969).
[12] D. W. Norcross, J. Phys. B: At. Mol. Phys. **4**, 1458 (1971).
[13] D. L. Moores, J. Phys. B: At. Mol. Phys. **19**, 1843 (1986).
[14] S. J. Buckman and C. W. Clark, Rev. Mod. Phys. **66**, 539 (1994).

[15] D. Leep and A. Gallagher, Phys. Rev. A **10**, 1082 (1974).
[16] B. Jaduszliwer, A. Tino, B. Bederson, and T. M. Miller, Phys. Rev. A **24**, 1249 (1981).
[17] T. F. O'Malley, L. Rosenberg, and L. Spruch, Phys. Rev. **125**, 1300 (1962).
[18] C. Pouchan and D. M. Bishop, Phys. Rev. A **29**, 1 (1984).
[19] C. Pan, A. F. Starace, and C. H. Greene, Phys. Rev. A **53**, 840 (1996).
[20] M. Marinescu, H. R. Sadeghpour, and A. Dalgarno, Phys. Rev. A **49**, 982 (1994).
[21] C. H. Greene, Phys. Rev. A **42**, 1405 (1990).
[22] M. Aymar, C. H. Greene, and E. Luc-Koenig, Rev. Mod. Phys. **68**, 1015 (1996).
[23] A. M. Frolov, M. B. Ruiz, and D. M. Wardlaw, Chem. Phys. Lett. **608**, 191 (2014).
[24] C. E. Moore, *Atomic Energy Levels as Derived from the Analysis of Optical Spectra – Hydrogen through Vanadium*, National Standard Reference Data Series, NSRDS-NBS 35 Vol. I (Reprint of NBS Circ. 467, Vol. I, 1949) (National Bureau of Standards, Washington, DC, 1971).
[25] H. Bachau, E. Cormier, P. Decleva, J. E. Hansen, and F. Martín, Rep. Prog. Phys. **64**, 1815 (2001).
[26] M. J. Seaton, Proc. Phys. Soc. **88**, 801 (1966).
[27] P. Goy, J. Liang, M. Gross, and S. Haroche, Phys. Rev. A **34**, 2889 (1986).
[28] C.-J. Lorenzen and K. Niemax, Phys. Scr. **27**, 300 (1983).
[29] R. Guérout, M. Aymar, and O. Dulieu, Phys. Rev. A **82**, 042508 (2010).
[30] J. C. Stewart and M. Rotenberg, Phys. Rev. **140**, A1508 (1965).
[31] C. D. H. Chisholm and U. Öpik, Proc. Phys. Soc. **83**, 541 (1964).
[32] G. Maroulis and D. M. Bishop, J. Phys. B: At. Mol. Phys. **19**, 369 (1986).
[33] J. Dellwo, Y. Liu, D. J. Pegg, and G. D. Alton, Phys. Rev. A **45**, 1544 (1992).
[34] M. Tarana and R. Čurík, Phys. Rev. A **93**, 012515 (2016).
[35] K. Baluja, P. Burke, and L. Morgan, Comput. Phys. Commun. **27**, 299 (1982).
[36] O. Zatsarinny, Comput. Phys. Commun. **174**, 273 (2006).
[37] J. Taylor, *Scattering Theory: The Quantum Theory of Nonrelativistic Collisions*, Dover Books on Engineering (Dover, New York, 2006).
[38] R. K. Nesbet, *Variational Methods in Electron-Atom Scattering Theory* (Plenum Press, New York, 1980).
[39] J. Tennyson, Phys. Rep. **491**, 29 (2010).
[40] H. Friedrich, *Theoretical Atomic Physics* (Springer, Berlin, 2006).
[41] M. Puchalski, D. Kędziera, and K. Pachucki, Phys. Rev. A **84**, 052518 (2011).
[42] A. U. Hazi, Phys. Rev. A **19**, 920 (1979).
[43] D. H. Glass, P. G. Burke, C. J. Noble, and G. B. Wöste, J. Phys. B: At. Mol. Opt. Phys. **31**, L667 (1998).
[44] D. W. Norcross, J. Phys. B: At. Mol. Phys. **2**, 1300 (1969).
[45] T. F. O'Malley, L. Spruch, and L. Rosenberg, J. Math. Phys. **2**, 491 (1961).
[46] W. Domcke, Phys. Rep. **208**, 97 (1991).